Electronic Supplementary Material (ESI) for ChemComm.

CO_2-induced gate-opening structural transition process of a porous coordination polymer revealed by solid-state ^{13}C NMR

Takuya Kurihara,*[a] Yue Souri,[a] Munehiro Inukai,[b] and Motohiro Mizuno*[a,c,d]

[a]Division of Material Chemistry, Graduate School of Natural Science and Technology, Kanazawa University, Kakuma-machi, Kanazawa, Ishikawa 920-1192, Japan

[b]Graduate School of Technology, Industrial and Social Sciences, Tokushima University, 2-1 Minami-Josanjima-Cho, Tokushima 770-8506, Japan

[c]Nanomaterials Research Institute, Kanazawa University, Kakuma-machi, Kanazawa, Ishikawa 920-1192, Japan

[d]Institute for Frontier Science Initiative, Kanazawa University, Kakuma-machi, Kanazawa, Ishikawa 920-1192, Japan

*E-mail: kurihara@se.kanazawa-u.ac.jp, mizuno@se.kanazawa-u.ac.jp

1. Sample Preparation

Materials:

$Zn(NO_3)_2 \cdot 6H_2O$, methanol (MeOH), *N*,*N*-dimethylformamide (DMF), and PtO_2 were purchased from FUJIFILM Wako Pure Chemical Corporation. 5-nitroisophthalic acid (NO_2-ipH_2) and isophthalic acid (ipH_2) were received from Tokyo Chemical Industry. 4,4'-bipyridyl (bpy) and deuterium oxide (D_2O) were obtained from Sigma Aldrich. All reagents were used without further purification.

Synthesis of $[Zn(NO_2\text{-ip})(bpy)]_n$ (CID-5):

CID-5 was prepared according to the literature.[1] A 20 mL DMF solution of $Zn(NO_3)_2 \cdot 6H_2O$ (1 mmol, 297 mg) and NO_2-ipH_2 (1 mmol, 220 mg) was added to a 20 mL MeOH solution of bpy (1 mmol, 156 mg). The mixture was heated at 70 °C for 24 h in a Teflon-lined autoclave. The obtained pale-yellow powder of CID-5 was washed with MeOH several times and dried under vacuum at 200 °C overnight to remove the guest molecules (MeOH and DMF) in the pore.

Synthesis of $[Zn(NO_2\text{-ip})_{0.94}(ip)_{0.06}(bpy)]_n$ (CID-5'):

CID-5' was prepared with the same procedure as CID-5 using 0.9 mmol NO_2-ipH_2 (190 mg) and 0.1 mmol ipH_2 (16.6 mg) instead of 1 mmol NO_2ipH_2. The mixing ratio of NO_2-ip and ip in CID-5' was examined by ^1H solution NMR and obtained to be 0.94:0.06.

Synthesis of deuterated bpy:

Deuteration of bpy was conducted according to the literature.[2] bpy (2 mmol, 310 mg), PtO_2 (0.1 mmol, 22.7 mg), and D_2O (10 mL) were heated at 230 °C for 12 h in a Teflon-lined autoclave. The acetone solution of the obtained mixture was filtered and evaporated to recrystallize deuterated bpy (bpy-*d*). The deuteration ratio of bpy-*d* was confirmed by ^1H solution NMR to be 99%.

Synthesis of $[Zn(NO_2\text{-ip})_{0.96}(ip)_{0.04}(bpy\text{-}d)]_n$ {CID-5'(bpy-*d*)}:

CID-5'(bpy-*d*) was prepared with the same procedure as CID-5' using bpy-*d*. The mixing ratio of NO_2-ip and ip was examined by ^1H solution NMR and obtained to be 0.96:0.04.

2. Measurement Conditions

Powder X-ray diffraction (PXRD) measurement:

PXRD measurements for characterization of the synthesized samples were performed on Bruker D8 ADVANCE eco with Cu K_α radiation at room temperature. Synchrotron PXRD patterns were recorded with a wavelength of 0.79932 Å at the BL02B2 beamline of SPring-8 (Hyogo, Japan). The sample powder packed into a 0.4 mm borosilicate glass capillary was inserted into a quartz cell for high-pressure gas atmosphere measurement.

Thermogravimetry analysis (TGA):

TGA data were collected with Rigaku Thermo plus EVO2 TG 8121 at a heating rate of 10 °C/min under N_2 gas flow.

CO_2 sorption measurement:

CO_2 adsorption isotherm of CID-5' was recorded with BELSORP-HP at 298 K.

Solid-state nuclear magnetic resonance (NMR):

Solid-state ^{1}H, ^{13}C, and ^{2}H NMR measurements were carried out on a JEOL JNM-ECA300 spectrometer at a 7 T superconductor magnet with a JEOL 4 mm double resonance magic-angle spinning (MAS) probe at room temperature. The samples were packed into a 4 mm homemade zirconia rotor for high-pressure gas MAS NMR and sealed in a homebuilt gas loading chamber under various CO_2 pressures.[3,4] The sample amounts packed were about 15–20 mg. ^{13}C-enriched CO_2 (^{13}C 99%) purchased from Cambridge Isotope Laboratories was used in the ^{13}C measurements for the dynamics analysis of adsorbed CO_2 to enhance its ^{13}C signal intensity. In the ^{1}H, ^{2}H, and ^{13}C measurements for the ^{1}H T_1 analysis, non-enriched CO_2 was used. ^{13}C single-pulse MAS experiment was performed with a ^{13}C 90° pulse width of 2.1 μs and a MAS rate of 4 kHz. For quantitative measurement, a relaxation delay was set to 5 times larger than ^{13}C T_1 of adsorbed CO_2. The number of scans was 8192 for 0.15 MPa and 256 for 0.29–0.78 MPa. ^{13}C static echo spectra were acquired with ^{13}C 90° and 180° pulse widths of 2.6 and 5.2 μs, respectively, and an echo interval of 50 μs. ^{13}C cross-polarization (CP)/MAS measurement was

conducted with ^{1}H and ^{13}C spin-lock pulse strengths of 60 and ~55 kHz, respectively, at a MAS rate of 5 kHz. A ramped amplitude spin-lock pulse was used for ^{13}C. All ^{13}C spectra were acquired under ^{1}H SPINAL-64 heteronuclear dipolar decoupling pulse irradiation[5] with a pulse strength of 100 kHz. ^{2}H static quadrupolar-echo spectra were observed using a ^{2}H 90° pulse width of 2.625 μs and an echo interval of 100 μs. The spectral fitting in the ^{13}C chemical shift anisotropy (CSA) analysis and the peak deconvolution of the ^{13}C CP/MAS spectra were performed using ssNAKE software.[6] The definition of the chemical shift parameters (isotropic chemical shift δ_{iso}, chemical shift anisotropy δ_{aniso}, and asymmetry parameter η) used in the fitting analysis is:

$$\delta_{iso} = \frac{1}{3}(\delta_{xx} + \delta_{yy} + \delta_{zz}),$$

$$\delta_{aniso} = \delta_{zz} - \delta_{iso},$$

$$\eta = \frac{\delta_{yy} - \delta_{xx}}{\delta_{aniso}},$$

where δ_{xx}, δ_{yy}, and δ_{zz} are the principal values of the chemical shift tensor and $|\delta_{zz} - \delta_{iso}| \geq |\delta_{xx} - \delta_{iso}| \geq |\delta_{yy} - \delta_{iso}|$. The errors in δ_{aniso} and η were estimated by comparing the experimental MAS spectra with calculated line shapes. Simulation of ^{13}C and ^{2}H line shapes under molecular motion was performed with a homebuilt Fortran program.[7]

Scanning electron microscopy (SEM):

SEM images were obtained using JEOL JSM-7610F FE-SEM with 15 kV voltage. The sample powder was mounted on a sample holder with carbon tape and sputtered with gold.

3. Figures and Tables

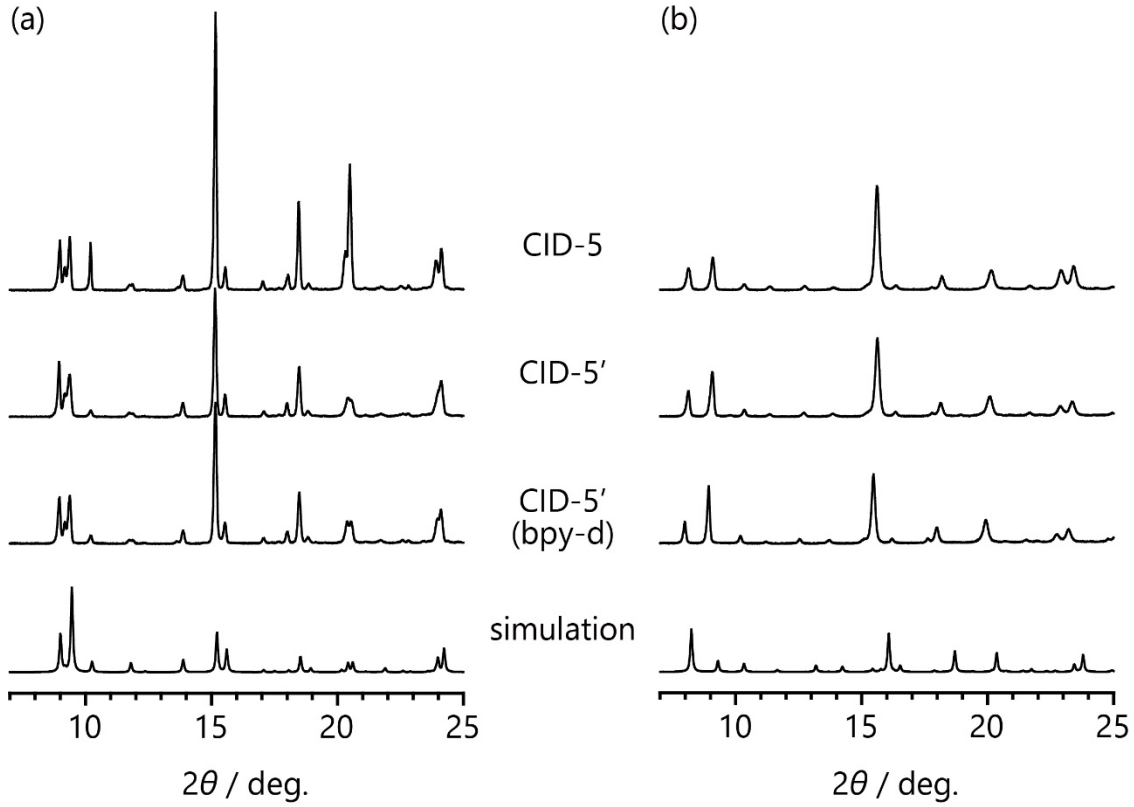

Figure S1. PXRD patterns of (a) as-synthesized CID-5, CID-5', and CID-5'(bpy-*d*), and (b) degassed ones. Simulated patterns of as-synthesized and degassed CID-5 are also shown.

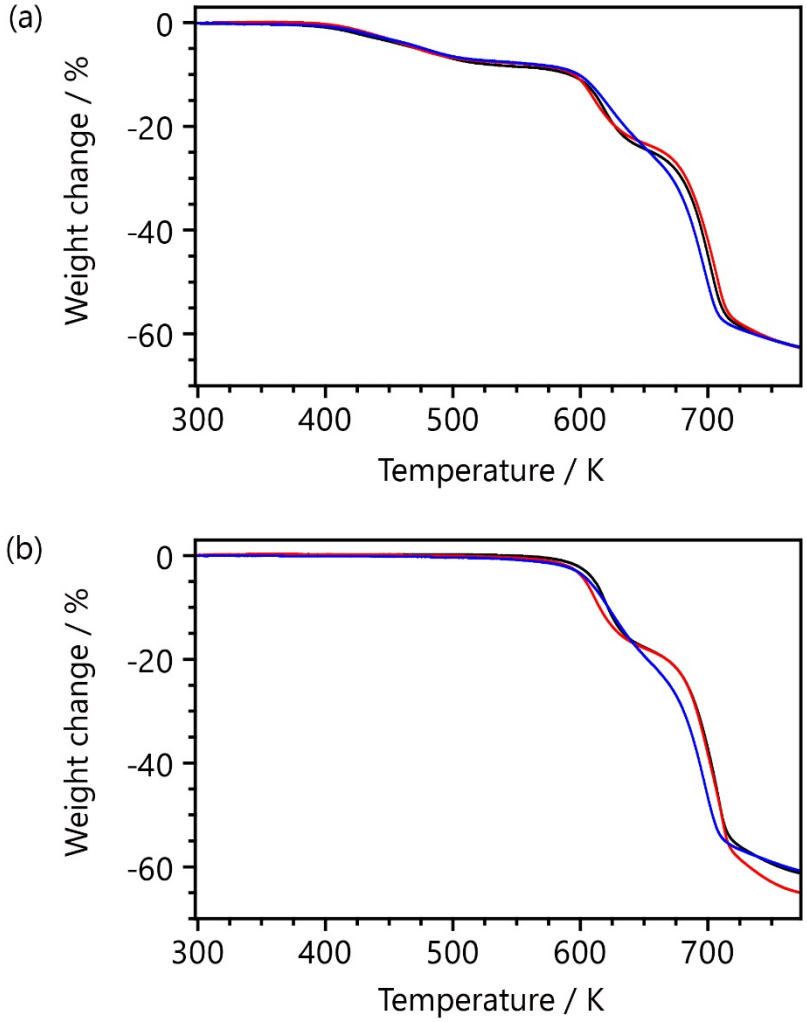

Figure S2. TGA profiles of (a) as-synthesized CID-5 (black), CID-5' (red), and CID-5'(bpy-*d*) (blue), and (b) degassed ones.

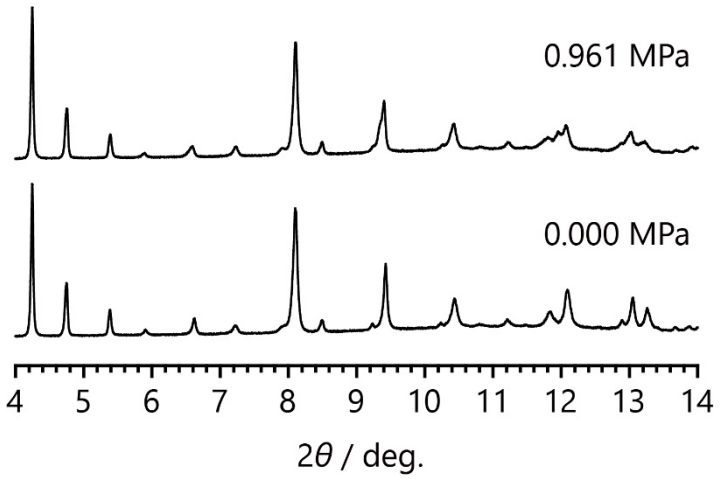

Figure S3. Synchrotron PXRD patterns of degassed CID-5 under 0.000 and 0.961 MPa CO_2 at 300 K. Similarity of the diffraction patterns indicates that the gate-opening structural transition of CID-5 occurs above 1 MPa at room temperature.

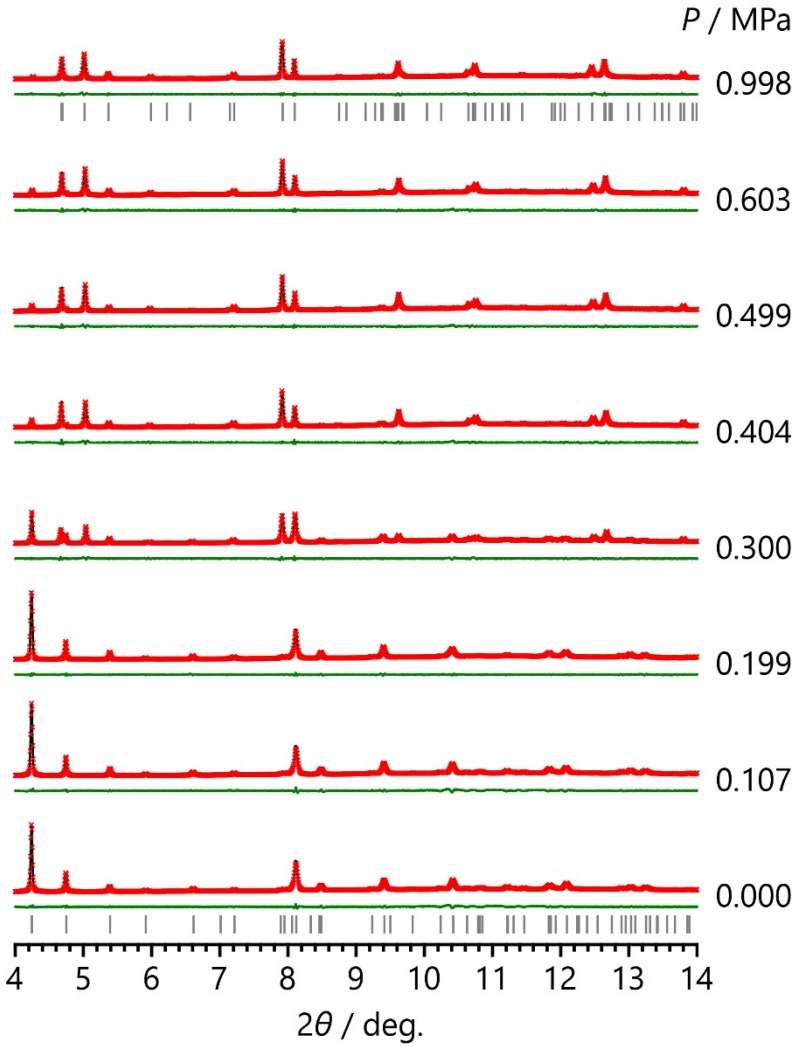

Figure S4. The results of the Le Bail fitting (red crosses) for the synchrotron PXRD patterns of CID-5' (black line) at 300 K. The difference of the fitting (green line) and Bragg positions (grey bars) are also shown. Peak search, indexing, and cell estimation of the diffraction patterns at 0.000 and 0.998 MPa were initially performed with EXPO2014 software.[8] The obtained cell parameters were refined by the Le Bail method on Jana2006 software.[9] In the analysis of the other diffraction patterns, the cell parameters of the structures at 0.000 and 0.998 MPa were used as the initial parameters and refined by the Le Bail fitting. The refined cell parameters are shown in Tables S1 and 2.

Table S1. Crystallographic data of the closed phase of CID-5' under various CO_2 pressures at 300 K.

P / MPa	0.000	0.107	0.199	0.300
Space group	P−1	P−1	P−1	P−1
a / Å	7.92130(18)	7.92491(17)	7.9266(3)	7.9162(4)
b / Å	10.1236(3)	10.1214(3)	10.1230(4)	10.1234(4)
c / Å	11.3949(4)	11.3898(4)	11.3923(4)	11.3906(5)
α / °	105.392(3)	105.392(3)	105.320(3)	105.379(5)
β / °	98.613(3)	98.646(2)	98.702(2)	98.824(4)
γ / °	95.8703(18)	95.92	95.871(3)	95.967(5)
V / Å^3	861.35(5)	861.24(4)	861.75(6)	859.64(7)
R_p	0.0260	0.0264	0.0202	0.0225
R_{wp}	0.0376	0.0377	0.0268	0.0324
GOF	2.42	2.47	2.22	2.69

P / MPa	0.404	0.499	0.603
Space group	P−1	P−1	P−1
a / Å	7.9138(4)	7.9157(4)	7.9160(3)
b / Å	10.1075(6)	10.1082(5)	10.1101(4)
c / Å	11.3924(5)	11.3926(4)	11.3881(5)
α / °	105.471(6)	105.459(4)	105.467(4)
β / °	98.996(4)	99.019(3)	99.035(3)
γ / °	95.380(6)	95.421(5)	95.443(4)
V / Å^3	858.62(8)	858.78(7)	858.50(6)
R_p	0.0235	0.0224	0.0220
R_{wp}	0.0347	0.0325	0.0317
GOF	2.87	2.70	2.63

Table S2. Crystallographic data of the open phase of CID-5' under various CO_2 pressures at 300 K.

P / MPa	0.300	0.404	0.499
Space group	P−1	P−1	P−1
a / Å	10.1178(3)	10.1100(5)	10.1055(5)
b / Å	10.0146(4)	10.0279(3)	10.0352(3)
c / Å	10.9306(6)	10.9280(5)	10.9259(5)
α / °	65.613(2)	65.589(2)	65.5889(17)
β / °	76.440(4)	76.373(4)	76.343(3)
γ / °	80.227(3)	80.217(4)	80.212(3)
V / Å^3	977.27(7)	977.16(8)	977.14(7)
R_p	0.0225	0.0235	0.0224
R_{wp}	0.0324	0.0347	0.0325
GOF	2.69	2.87	2.70

P / MPa	0.603	0.998
Space group	P−1	P−1
a / Å	10.1027(3)	10.1088(3)
b / Å	10.0420(3)	10.0712(3)
c / Å	10.9156(4)	10.9127(4)
α / °	65.5787(15)	65.5447(12)
β / °	76.383(3)	76.385(3)
γ / °	80.147(3)	80.069(3)
V / Å^3	976.57(6)	979.37(6)
R_p	0.0220	0.0212
R_{wp}	0.0317	0.0300
GOF	2.63	2.50

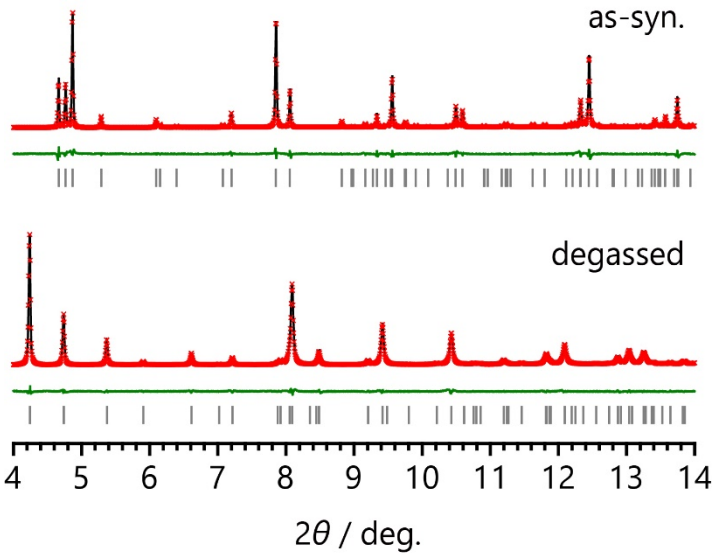

Figure S5. The results of the Le Bail fitting (red crosses) for the synchrotron PXRD patterns of CID-5 (black line) at 300 K. The difference of the fitting (green line) and Bragg positions (grey bars) are also shown. Peak search, indexing, and cell estimation of the diffraction patterns were performed with EXPO2014 software. The obtained cell parameters were refined by the Le Bail method on Jana2006 software and are summarized in Table S3. The refined cell parameters of the degassed closed form well agree with those of the closed form of CID-5', confirming that the crystal structure of CID-5' is similar to that of CID-5. Moreover, the parameters of the as-synthesized open form are similar to those of the CO_2-loaded open form of CID-5', suggesting a structural similarity between the two.

Table S3. Crystallographic data of CID-5 at 300 K.

P / MPa	As-syn.	Degassed
Space group	P−1	P−1
a / Å	10.1269(9)	7.92771(10)
b / Å	10.42897(13)	10.14380(17)
c / Å	10.74464(13)	11.40787(19)
α / °	65.0038(5)	105.6159(16)
β / °	77.0374(9)	98.5340(13)
γ / °	79.4244(10)	95.6068(10)
V / Å^3	997.48(2)	864.57(2)
R_p	0.0429	0.0347
R_{wp}	0.0637	0.0456
GOF	3.13	2.40

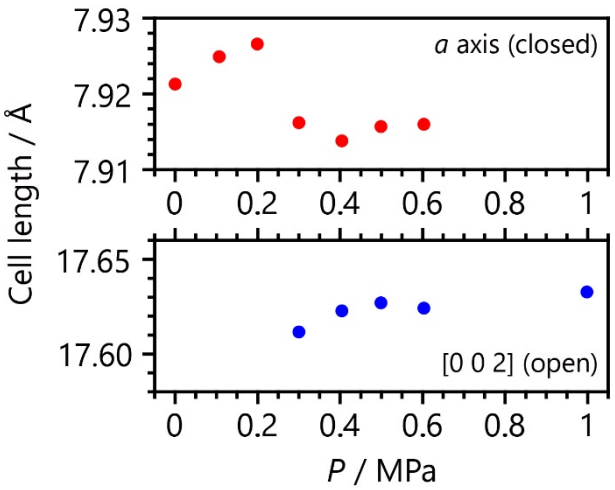

Figure S6. The inter-2D-layer distance of the closed- (the *a*-axis length) and open-phase (the [0 2 2] length) structures of CID-5' (red and blue, respectively).

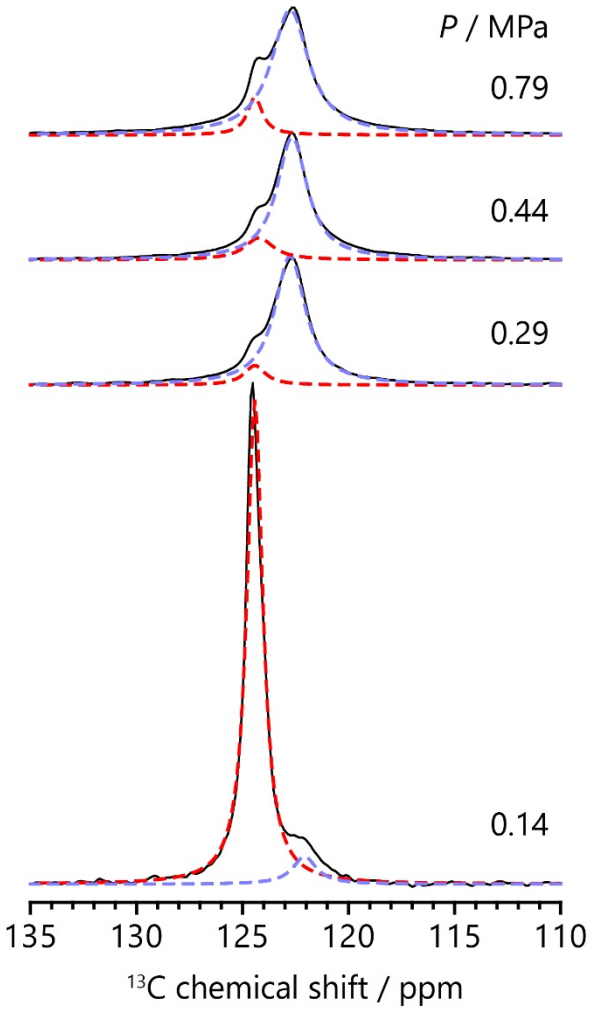

Figure S7. ^{13}C 1-pulse MAS spectra expanded around the center-band signal of 99% ^{13}C-enriched CO_2 ($^{13}CO_2$) adsorbed in CID-5'. The fitting results are also shown with colored dotted lines: light blue, adsorbed $^{13}CO_2$; red, gaseous $^{13}CO_2$ outside the MOF crystalline particles. Signals from the ligands were not observed in the spectra due to the low ^{13}C natural abundance (1%) and long ^{13}C T_1 relaxation times.

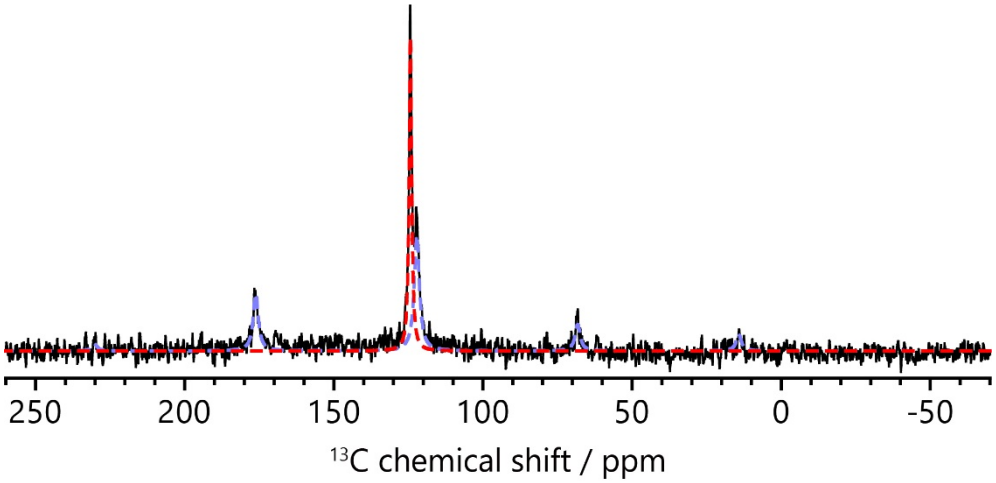

Figure S8. ^{13}C MAS spectrum of $^{13}CO_2$ adsorbed in CID-5' under 0.14 MPa $^{13}CO_2$ at room temperature. The MAS rate was 4 kHz. The fitting result is also shown (adsorbed $^{13}CO_2$, light blue; gaseous $^{13}CO_2$, red). The CSA parameters of adsorbed $^{13}CO_2$ at 0.14 MPa were not used in the analysis of the CO_2 dynamics because of the lower signal-to-noise ratio of the spectrum compared to that at 0.15 MPa.

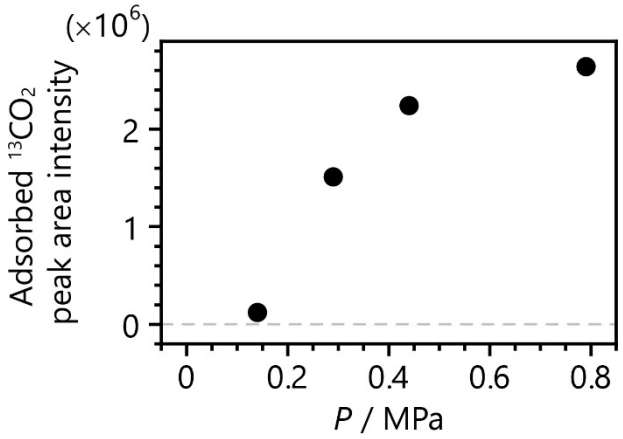

Figure S9. The pressure dependence of the ^{13}C peak area intensity of adsorbed $^{13}CO_2$. The peak area intensity at 0.14 MPa $^{13}CO_2$ pressure was used in this plot instead of that at 0.15 MPa because the sample amount used in the measurement at 0.15 MPa was different from that at the other pressures. The ^{13}C T_1 relaxation times of adsorbed $^{13}CO_2$ were 0.41 (0.14 MPa), 1.44 (0.29 MPa), 1.84 (0.44 MPa), and 2.04 s (0.79 MPa). The $^{13}CO_2$ signals were acquired with relaxation delays 5 times larger than the T_1 values.

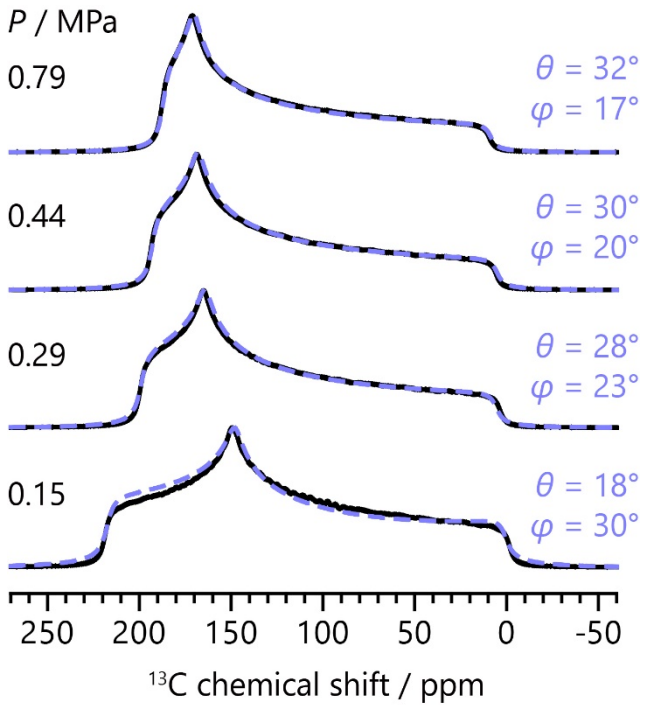

Figure S10. The analysis results of the ^{13}C CSA line shapes of adsorbed $^{13}CO_2$. Black lines were calculated using the CSA parameters obtained by fitting the ^{13}C MAS sideband pattern of adsorbed $^{13}CO_2$ (shown in Table 1 in the main text). The simulation analysis was performed using the calculated static spectra. Light blue dotted lines are the best-fit line shapes simulated under the combination of 6-site rotation with the tilting angle θ and 2-site flipping with the angle φ at the fast motion limit (>10^6 Hz). The ^{13}C CSA parameters of solid CO_2, $\delta_{aniso} = -223$ ppm and $\eta = 0$, were used in the simulation.[10]

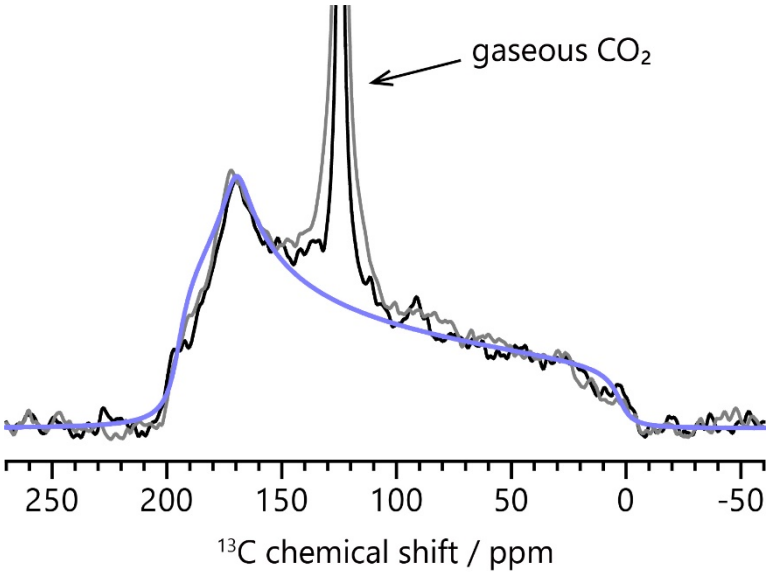

Figure S11. The analysis results of the ^{13}C CSA line shape of adsorbed $^{13}CO_2$. Black and grey lines are ^{13}C echo spectra of $^{13}CO_2$ adsorbed in CID-5' recorded at 0.29 and 0.78 MPa, respectively, without MAS. A light blue line is the best-fit simulated line shape calculated with the tilting angle $\theta = 29°$ and the flipping angle $\varphi = 20°$. The detail of the spectral simulation method is shown in the caption of Figure S10. Comparing the motional angles obtained from the MAS and static spectra at 0.29–0.79 MPa indicates that the MAS analysis involves deviations of $\theta \approx \pm 2°$ and $\varphi \approx \pm 3°$.

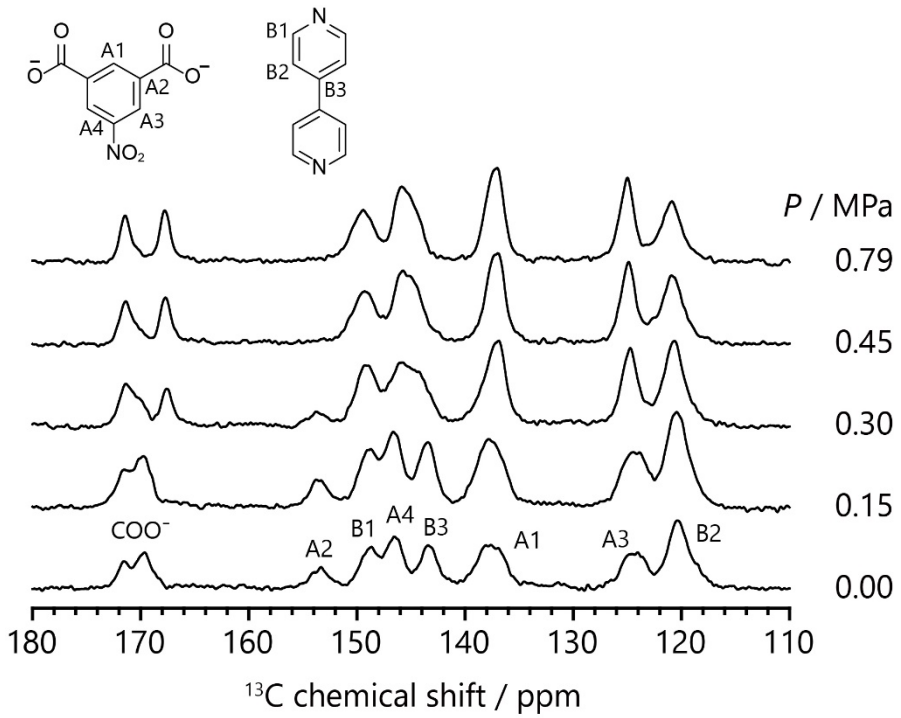

Figure S12. ^{13}C CP/MAS NMR spectra of CID-5' under different $^{13}CO_2$ pressures with a CP contact time of 2 ms at a MAS rate of 5 kHz. The peaks were assigned based on CP contact time dependences of the signals and ^{13}C solution NMR spectra of the ligands. The spectral change depending on the pressure is attributed to the structural transition. No observation of the $^{13}CO_2$ signal is caused by the fast $^{13}CO_2$ diffusion in the pore because such motion averages out ^{1}H–^{13}C dipolar interactions between the ligand protons and adsorbed $^{13}CO_2$, which disturbs the dipolar-based CP magnetization transfer. This result is consistent with the presence of the fast CO_2 hopping motion (>10^6 Hz) revealed by the CSA analysis because continuous hopping motion through the pore results in the diffusional motion.

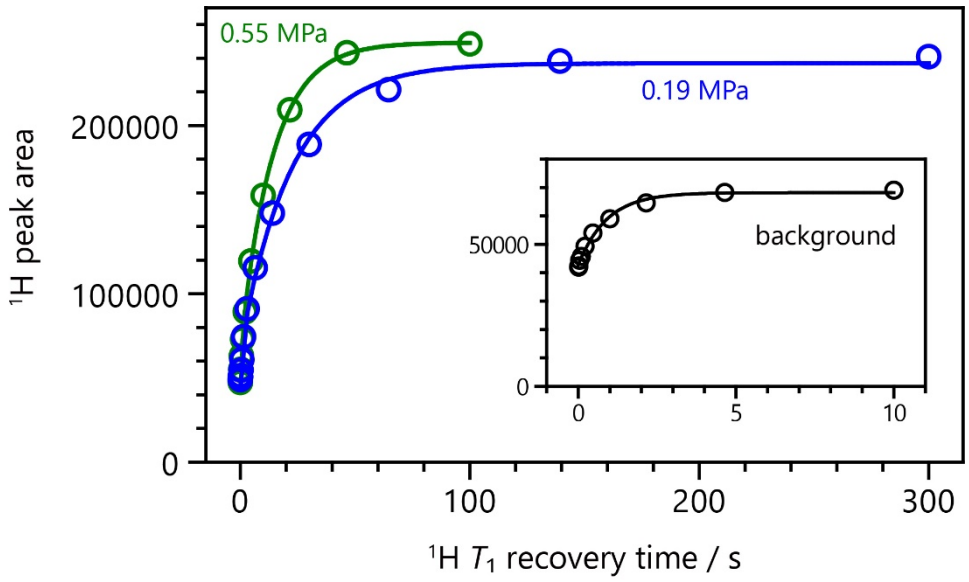

Figure S13. The least-squares fitting results of the ^{1}H T_1 saturation recovery experiments at 0.19 (blue) and 0.55 (green) MPa CO_2 pressures before starting and after completing the gate-opening transition, respectively. Signals from a spinning cap of the MAS rotor and a MAS module around a detection coil were also detected in the experiments. In addition, the latter could not be removed by the pre-saturation pulses of the T_1 measurement. To consider the influence of these background signals on the T_1 fitting analysis, we used the double-exponential function:

$$M^{CID}\left[1-\exp\left(-t/T_1^{CID}\right)\right]+M^{BG}\left[1-\exp\left(-t/T_1^{BG}\right)\right]+C$$

where M^x (x = CID, BG) and $T_1{}^x$ are the magnetization in the thermal equilibrium state and the T_1 value of CID-5' and background (spinning cap), respectively, and C is the residual background signal (MAS module). M^{BG}, $T_1{}^{BG}$, and C were determined to be 2.553 (±0.091) × 10^4, 0.9045 (±0.1011) s, and 4.272 (±0.061) × 10^4 by the T_1 measurement with an empty MAS NMR rotor (the inset in Fig. S13) and used as the constant values in the T_1 analysis of CID-5'. M^{CID} and $T_1{}^{CID}$ were used as the fitting parameters in the analysis.

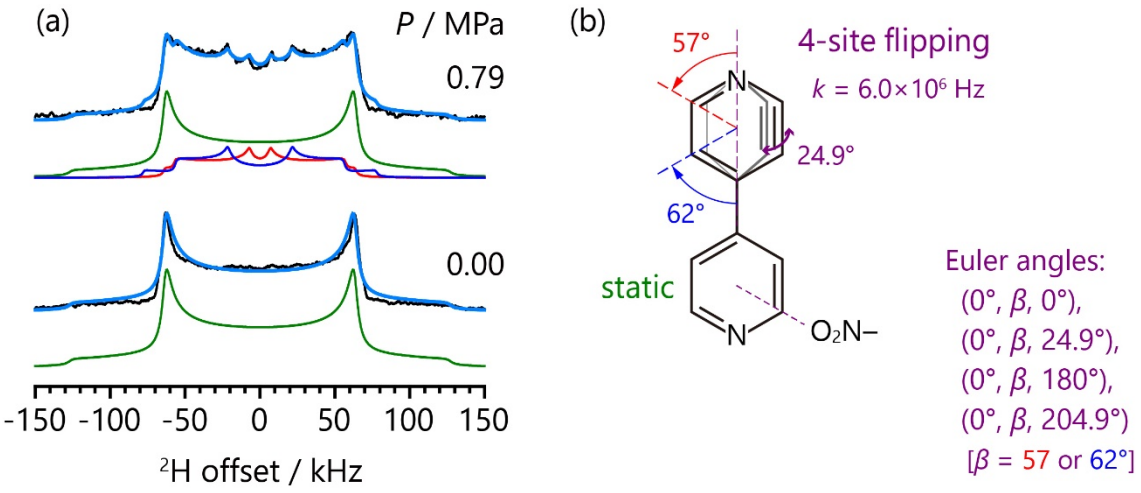

Figure S14. (a) ^{2}H quadrupolar-echo NMR spectra of CID-5'(bpy-*d*) at 0.00 and 0.79 CO_2 pressures (black). The ^{2}H NMR study in the previous work revealed that one of the two pyridyl rings of bpy in the as-synthesized open form of CID-5 undergoes four-site flipping and the other one has no motion and that the two pyridyl rings in the degassed closed-form show no motion.[11] According to this report, we analyzed the ^{2}H spectra of CID-5'(bpy-*d*) by ^{2}H line shape simulation with a quadrupolar coupling constant of 169 kHz and an asymmetry parameter of 0. The detailed structural model used in the simulation is shown in (b). The presence of the two different orientation angles 57° and 62° to the rotation axis in bpy is based on the crystal structure of the as-synthesized open form of CID-5. The best-fit line shapes to the experimental spectra are shown with light blue lines. The spectrum at 0.00 MPa (closed form) was well reproduced with the simulated pattern under no motion (green). The simulation result at 0.79 MPa (open form) is the sum of the three line shapes calculated under two four-site flipping motions with the motional rate k_{flip} of 6.0 × 10^6 Hz and the orientation angles of 57 and 62° (red and blue, respectively) and no motion at the ratio of 0.5:0.5:1. This value corresponds to the presence of the rotating and static pyridyl rings of bpy with the ratio 1:1, which agrees with the ^{2}H NMR result in the previous work.

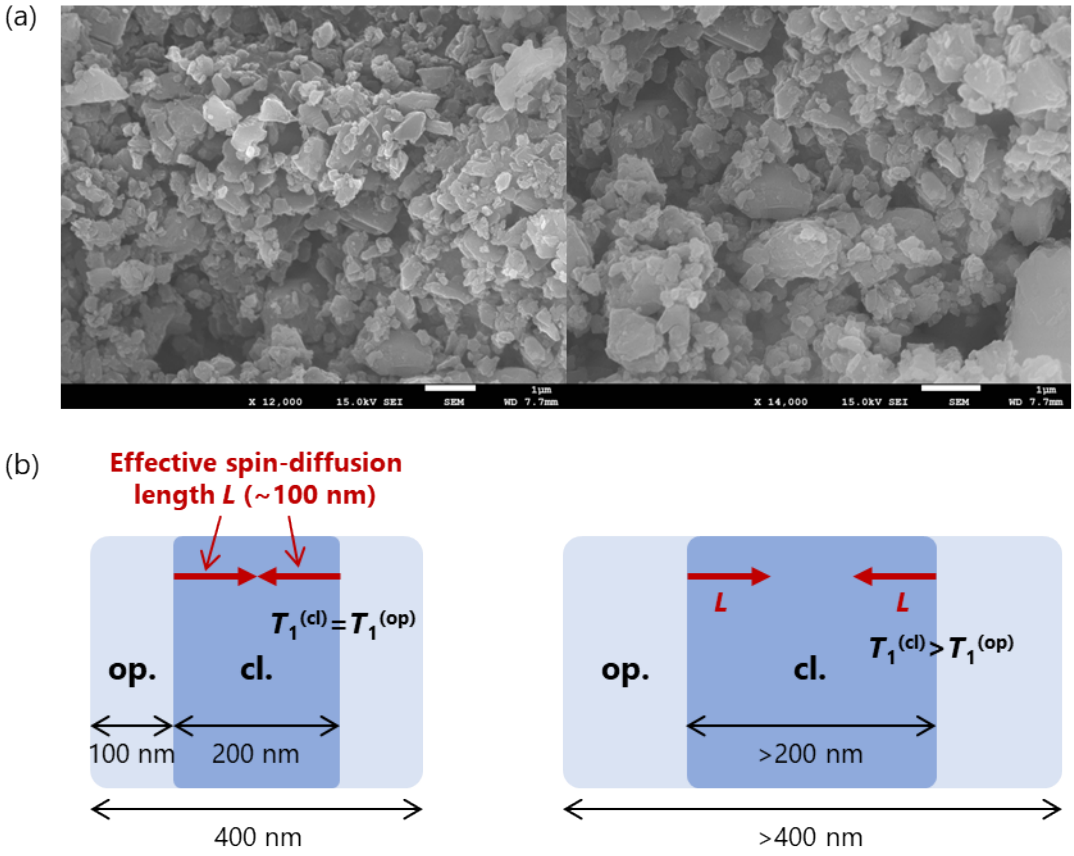

Figure S15. (a) SEM images of CID-5' microcrystalline particles. The particle size is distributed in the order of 10^2 nm. The effective spin-diffusion length L is estimated to be about 100 nm using the diffusion equation and ^{1}H T_1 of the open phase at 0.55 MPa (14.2 s). When the transition occurs from the crystal surface of the closed structure, crystalline particles of 2D layered CID-5' probably form a sandwich-like structure in the intermediate state during the transition as shown in (b). We performed the T_1 analysis at 0.28 MPa, at which the adsorption isotherm (Fig. 1b) and ^{13}C peak area intensity of adsorbed CO_2 (Fig. S9) indicate about half part of a CID-5' crystal forms the open structure. In this structural model, therefore, ^{1}H T_1 of the closed phase in crystalline particles with up to ~400 nm diameter becomes the same value as that of the open phase owing to the effect of ^{1}H spin diffusion. On the other hand, ^{1}H T_1 of the closed phase in particles with over ~400 nm diameter becomes longer compared to that of the open phase as particle size increases. As a result, ^{1}H T_1 of the closed phase in the entire crystalline particles would become longer than that of the open phase and possess a distribution. Compared with the closed phase below the gate-opening pressure, ^{1}H T_1 of the closed phase in this intermediate-state model becomes shorter with a distribution.

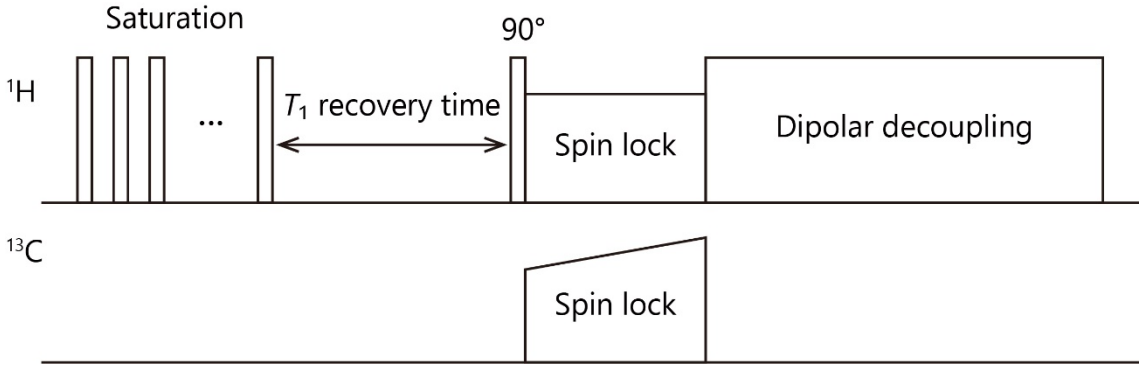

Figure S16. Pulse sequence of ^{13}C CP/MAS-detected ^{1}H T_1 saturation recovery experiment.

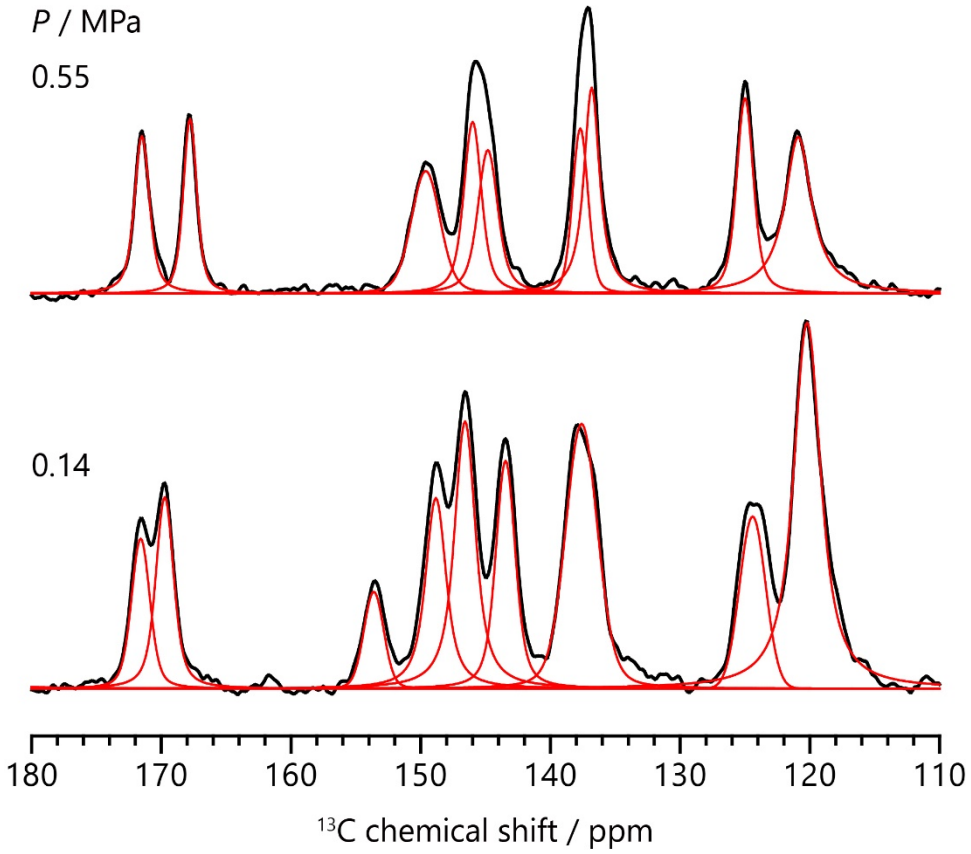

Figure S17. ^{13}C CP/MAS spectra of CID-5' at 0.14 and 0.55 MPa CO_2 pressures, corresponding to the closed and open phases, respectively, with a CP contact time of 5 ms at a MAS rate of 5 kHz. The results of the peak deconvolution by the spectral fitting are shown with red lines. The obtained line shape parameters were used for the deconvolution of the ^{13}C CP/MAS spectra at 0.28 MPa as shown in Fig. S18.

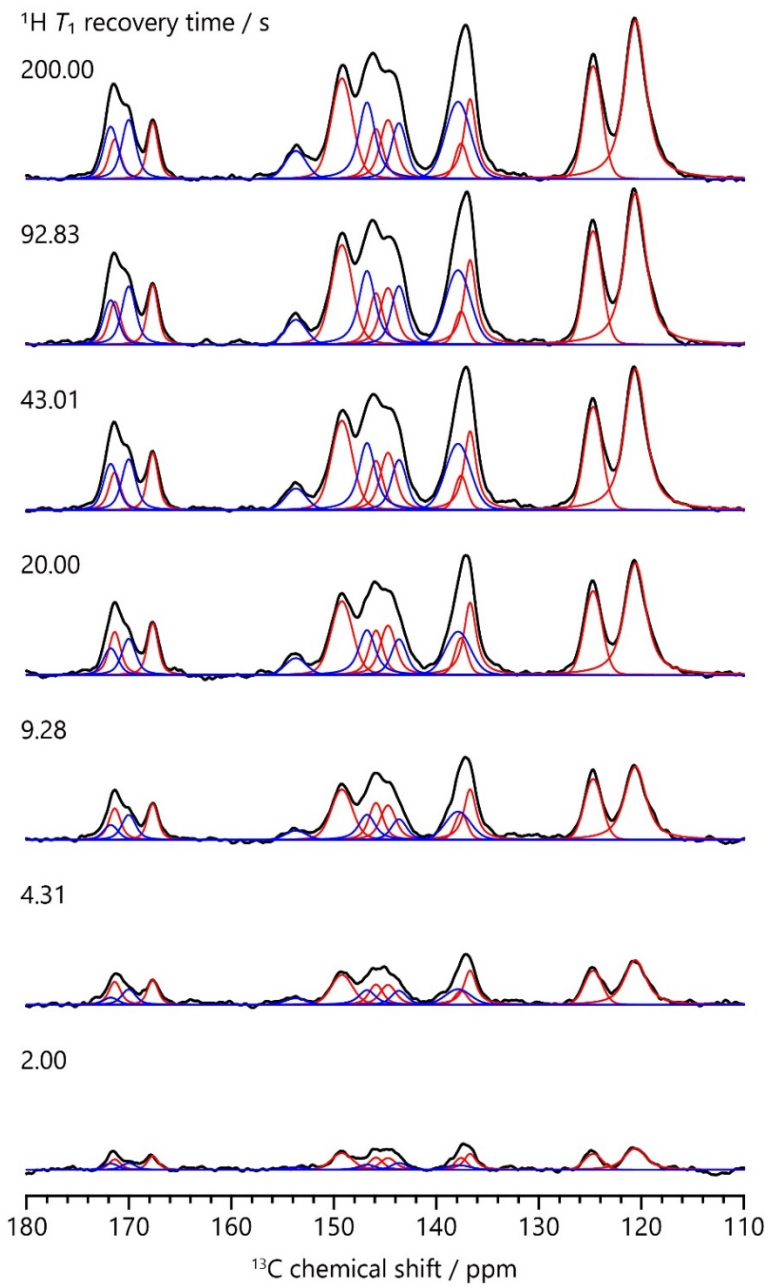

Figure S18. ^{13}C spectra of CID-5' at 0.28 MPa CO_2 pressure obtained by the ^{13}C CP/MAS-detected ^{1}H T_1 saturation recovery experiment with a CP contact time of 5 ms at a MAS rate of 5 kHz. The results of the peak deconvolution by spectral fitting are also shown with colored lines. The fitting was performed based on the results of peak deconvolution of the ^{13}C CP/MAS spectra at 0.14 and 0.55 MPa (Fig. S17). The peaks shown with blue lines are the signals from the closed structure, and the sum of their area intensities was used for the T_1 analysis. The signals at 120.8, 124.8, and 149.2 ppm could not be decomposed into the closed- and open-phase peaks due to the large overlapping of the two components.

4. References

(1) T. Fukushima, S. Horike, Y. Inubushi, K. Nakagawa, Y. Kubota, M. Tanaka and S. Kitagawa, *Angew. Chem.*, *Int. Ed.*, 2010, **49**, 4820–4824.

(2) M. Yamamoto, K. Oshima and S. Matsubara, *Heterocycles*, 2006, **67**, 353–359.

(3) M. Inukai, T. Kurihara, Y. Noda, W Jiang, K. Takegoshi, N. Ogiwara, H. Kitagawa and K. Nakamura, *Phys. Chem. Chem. Phys.*, 2020, **22**, 14465–14470.

(4) T. Kurihara, M. Inukai and M. Mizuno, *J. Phys. Chem. Lett.*, 2022, **13**, 7023–7028.

(5) B. M. Fung, A. K. Khitrin and K. Ermolaev, *J. Magn. Reson.*, 2000, **142**, 97–101.

(6) S. G. J. van Meerten, W. M. J. Franssen and A. P. M. Kentgens, *J. Magn. Reson.*, 2019, **301**, 56–66.

(7) M. Mizuno, A. Iwasaki, T. Umiyama, R. Ohashi and T. Ida, *Macromolecules*, 2014, **47**, 7469–7476.

(8) A. Altomare, C. Cuocci, C. Giacovazzo, A. Moliterni, R. Rizzi, N. Corriero and A. Falcicchio, *J. Appl. Cryst.*, 2013, **46**, 1231–1235.

(9) V. Petříček, M. Dušek and L. Palatinus, *Z. Kristallogr.*, 2014, **229**, 345–352.

(10) A. J. Beeler, A. M. Orendt, D. M. Grant, P. W. Cutts, J. Michl, K. W. Zilm, J. W. Downing, J. C. Facelli, M. S. Schindler and W. Kutzelnigg, *J. Am. Chem. Soc.*, 1984, **106**, 7672–7676.

(11) M. Inukai, T. Fukushima, Y. Hijikata, N. Ogiwara, S. Horike and S. Kitagawa, *J. Am. Chem. Soc.*, 2015, **137**, 12183–12186.